



# Improving edge quality and optical transmittance of Ag films on glass substrates by selective nanosecond pulsed laser ablation using various scanning methods

Baojia Li<sup>1,4</sup> · Huang Li<sup>1,4</sup> · Lijing Huang<sup>2,3,4</sup> · Yilun Wang<sup>3,4</sup> · Shuangshuang Li<sup>3,4</sup> · Naifei Ren<sup>3,4</sup>

Received: 11 March 2019 / Accepted: 24 June 2019 / Published online: 27 June 2019  
© Springer Science+Business Media, LLC, part of Springer Nature 2019

## Abstract

Selective laser ablation (SLA) of silver (Ag) films, which were deposited on glass substrates by radio frequency (RF) magnetron sputtering, was performed by using a 532 nm nanosecond (ns) pulsed laser. Two kinds of simple and mask-free SLA strategies featured by two new scanning paths (i.e. frame-typed serial scanning, FTSS, and frame-line combined scanning, FLCS) were proposed to improve the edge quality and optical transmittances of the SLA patterns. The effects of laser scanning speed ( $v$ ), hatch distance ( $HD$ ) and scanning path on edge quality of the laser-ablated grooves and SLA patterns were systematically studied. The results indicated that compared with the conventional line-typed cyclic scanning (LTCS) path, which resulted in unsmooth edge with semicircle-shaped boundaries and some Ag residues, the proposed scanning paths of FTSS and FLCS produced clean and smooth edges without obvious heat-affected zone and Ag residues under the condition of using a  $v$  value of 15 mm/s and an  $HD$  value of 90  $\mu\text{m}$ . As a result, the as-obtained SLA patterns exhibited relatively high optical transmittances. The simple methods of adopting the FTSS or FLCS path for improving the edge quality during SLA and thus the optical transmittance of SLA patterns may have great potential application in various fields.

## 1 Introduction

Recently, patterning of metal films by selective laser ablation (SLA) has been widely studied, which can be applied in fabrication of microelectrodes [1, 2], film transistors [3, 4], radio frequency identification (RFID) antennas [5], organic light emitting devices (OLED) [6, 7] and solar cells [8–10] owing to its advantages of high processing efficiency and high flexibility in pattern choice. In general, laser ablation or removal of metal films is a photo-thermal process in which light energy gets absorbed by free electrons in the

metals [11, 12]. Consequently, desired clean patterns can be obtained due to the local heating and material removal [13, 14].

Femtosecond (fs) and picosecond (ps) lasers have been widely utilized as SLA tools for accurate material removal owing to their advantages of ultrashort pulse duration, almost no heat-affected zone etc. [1, 11, 14–16]. However, they are still hard for application in practical industrial production such as laser cleaning and laser polishing as a result of their inherent deficiencies such as high device cost and low removal efficiency. Different from fs and ps laser sources, the nanosecond (ns) laser source is industrially friendly and adaptable and can deliver high throughput processes [17]. In the mask-assisted ns laser patterning process, the laser beam was spatially modulated through a photomask in contact with the front side or the back side of the substrate and then made incident into the metal film [18–20]. The metal film was detached from the substrate under the pulsed laser-induced thermo-elastic force which could shear along the weakly bonded grain boundary regions [18]. As a consequence, high-fidelity patterns with good edge quality at the micrometer scale would be fabricated. However, this method needs the introduction

✉ Baojia Li  
li\_bjia@126.com

<sup>1</sup> School of Materials Science and Engineering, Jiangsu University, Zhenjiang 212013, People's Republic of China

<sup>2</sup> Institute of Micro-Nano Optoelectronic and Terahertz Technology, Jiangsu University, Zhenjiang 212013, People's Republic of China

<sup>3</sup> School of Mechanical Engineering, Jiangsu University, Zhenjiang 212013, People's Republic of China

<sup>4</sup> Jiangsu Provincial Key Laboratory of Center for Photon Manufacturing Science and Technology, Jiangsu University, Zhenjiang 212013, People's Republic of China

of a mask whose preparation process is complex and the transparent substrate for backside patterning.

It is also interesting to note that the laser scanning path has significant influences on the edge quality of SLA patterns. The line-by-line round-trip cyclic scanning (i.e. line-typed cyclic scanning, LTCS) was noticed to be the most commonly used scanning path in previous studies [21–23]. Romoli et al. [21] succeed in ablating an area of 10 mm × 10 mm on a ceramic coating deposited on the bottom surface of a soda-lime glass substrate by using this scanning path. However, the edge of the pattern was unsmooth and some material residues occurred on the surface. By using this scanning path, Tang et al. [22] fabricated highly organized periodic microstructures on a copper substrate and found semicircle edges at the start and end points of laser scanning. Richards et al. [23] reported that plenty of cracks could be generated by using this conventional LTCS method. Although desired patterns could be obtained by using the scanning path of the conventional LTCS, the edge quality of the pattern was usually poor. The poor edge quality would lead to significantly degraded device performance, such as the efficiency of solar cells and the service performance of aerial antennas. Until now, the most commonly used materials for preparing metal patterns are silver (Ag), copper (Cu) and gold (Au), which should be attributed to their higher electrical conductivity [19]. However, the high material cost of Au is not conducive to practical production and application, and Cu is easily oxidized in air that will finally result in a decrease in electrical conductivity [17]. In contrast, Ag has relatively lower resistivity and better air stability than Cu. Hence, the mask-free SLA of Ag films by ns pulsed laser involving change of the scanning path and process parameters to improve the edge quality and the related performance is still worth studying.

In this work, two kinds of simple and mask-free SLA strategies featured by two new scanning paths (i.e. framed serial scanning, FTSS, and frame-line combined scanning, FLCS) were proposed to improve the edge quality and the optical transmittance of the selective ns pulsed laser-ablated grooves and patterns. Specifically, Ag films deposited on glass substrates by radio frequency (RF) magnetron sputtering were selectively ablated by a 532 nm ns pulsed laser using these two new scanning paths (i.e. FTSS and FLCS) and the conventional scanning path (i.e. LTCS). The effects of laser scanning speed ( $v$ ), hatch distance ( $HD$ , the distance between two adjacent grooves [17, 21, 22]) and scanning path on edge quality of laser-ablated grooves and SLA patterns were systematically investigated, and the effect of scanning path on optical transmittance of SLA patterns was analyzed. The availabilities of the proposed strategies were confirmed by comparing the results of FTSS and FLCS with those of LTCS.

## 2 Experimental

The commercial soda-lime float glass (Shenzhen Nuozech Technology Co., Ltd., China) with a size of 15 mm × 15 mm and a thickness of about 1.0 mm was chosen as the substrate and cleaned in deionized water, acetone and anhydrous ethanol by ultrasonic bath. The cleaning time for each process was set to 10 min. The substrate was dried by blowing high-purity (99.99%) nitrogen after the ultrasonic cleaning.

Ag films with thicknesses of 100 nm were deposited on the pre-cleaned glass substrates by RF magnetron sputtering at room temperature using an Ag target [Zhongnuo Advanced Material (Beijing) Technology Co., Ltd., China, 99.99% purity]. During sputtering deposition, the distance between the substrates and the target was fixed to 50 mm, and the sputtering gas was high-purity (99.999%) argon. The RF power, the working pressure and the rotation speed of the sample stage were tuned to 30 W, 4 Pa and 4 r/min, respectively. The thicknesses of the Ag films were monitored by a quartz-crystal-based thickness monitor which was provided by the RF magnetron sputtering deposition system (Hefei Kejing Materials Technology Co., Ltd., China, VTC-2RF).

A diode pumped Nd:YVO<sub>4</sub> ns pulsed laser (Bright Solution Co., Ltd., Italy, Wedge532) with a central wavelength of 532 nm was used for SLA of Ag films. The pulse width, the repetition rate and the max single pulse energy of the ns pulsed laser were 1–2 ns, 1 kHz and 0.9 mJ, respectively. Figure 1 shows the schematic diagram of the ns pulsed laser ablation system. The system was consisted of a beam expander, a total reflector, a vibrating mirror system (Raylase AG Co., Ltd., Germany, Supscan-15) and a focusing lens (with a focal length of 20 cm). In the vibrating mirror system, the defocusing amount could be adjusted from +15 to –15 mm in Z-direction by a computer software. The samples placed on the X–Y moving stage could realize

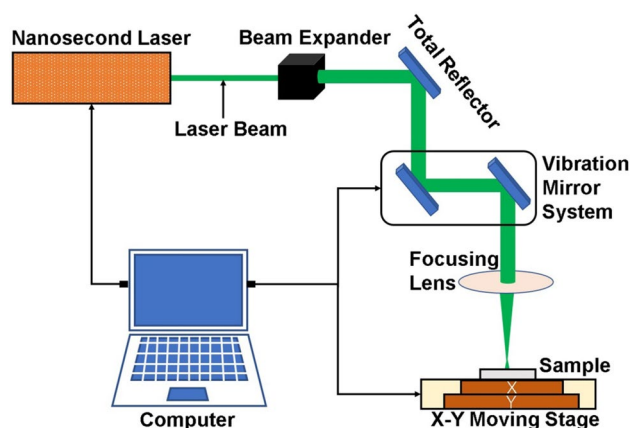


Fig. 1 Schematic diagram of the nanosecond pulsed laser ablation system

two-dimensional motions controlled by the computer software. Some reports showed that a significant thermal influence would generate by adopting a small defocusing amount and a high pulse energy density [5, 11]. Therefore, the surfaces of Ag films were located after the focal spot of the laser beam with a defocusing amount of 1.0 mm and the laser fluence was set to 0.8 J/cm<sup>2</sup>. In order to obtain grooves or patterns with good edge quality, different  $v$  and  $HD$  values as well as scanning paths (i.e. LTCS, FTSS and FLCS) were set and controlled by the computer software. The quality of single-groove laser ablation for preparing patterns was firstly studied in the following experiment owing to the fact that the quality of the SLA pattern was determined by the quality of the single SLA groove.

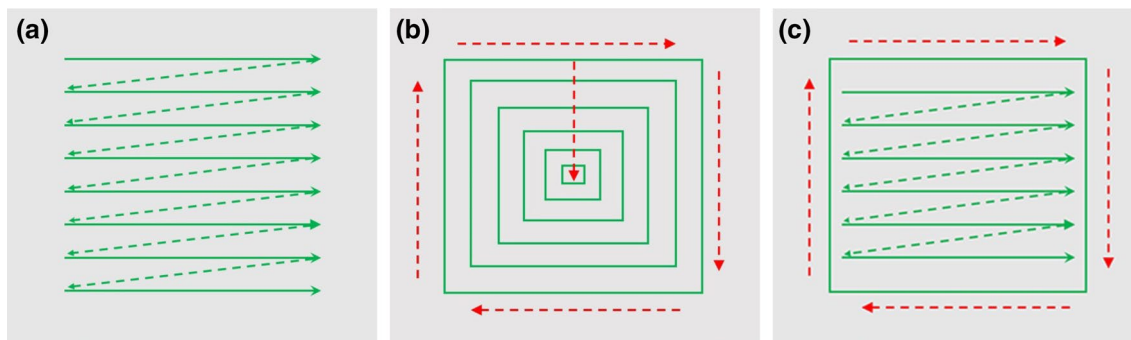
Figure 2 shows the schematic diagram of the three different scanning paths adopted in the present study. Figure 2a shows the schematic diagram of the conventional LTCS which consists of parallel lines. The laser scanning direction was set to be single direction along the parallel lines. Figure 2b shows the schematic diagram of the FTSS which consists of a plurality of squares or rectangles with different sizes. The laser scanning direction was set to be along the squares or rectangles from outside to inside. Figure 2c shows the schematic diagram of the FLCS which consists of a plurality of parallel lines and a square or rectangle that

surrounds the parallel lines. The laser scanning direction was set to be single direction along the parallel lines inside at first and then along the outer square or rectangle.

A confocal laser scanning microscope (CLSM) (Keyence Corp., Japan, VK-X260K) was used to provide both optical image and three-dimensional profiles of the samples. The surface morphology was observed by a scanning electron microscope (SEM) (Hitachi Corp., Japan, S-3400N). An energy dispersive X-ray (EDX) spectrometer (EDAX Inc., USA, E550) was used to analyze the chemical composition changes of the samples. A UV–Vis spectrophotometer (Shanghai Metash Instruments Co., Ltd., China, UV-8000) was used to characterize the optical transmittances of the samples.

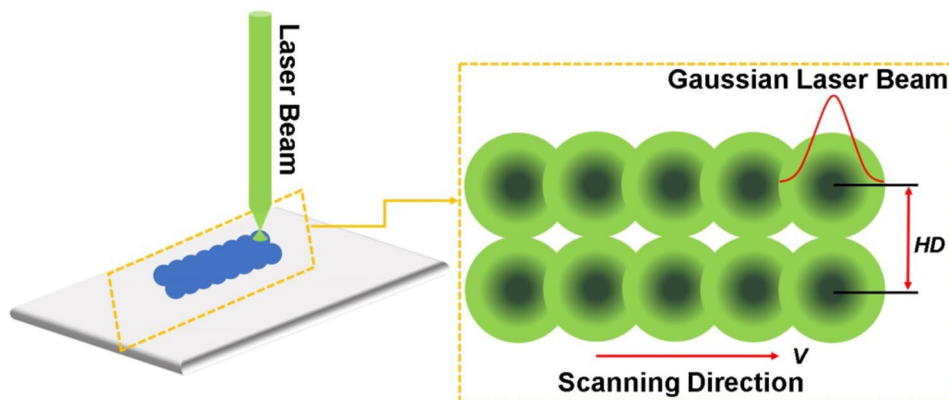
### 3 Results and discussion

Figure 3 shows the schematic diagram of the laser scanning parameters. The ns pulsed laser beam follows a Gaussian distribution. According to the path drawn by the computer software coupled with the control of the  $v$  and  $HD$  values, desired patterns with good edge quality and less material residues can be generated by multi-pulse stacking ns laser ablation [24]. Here, in order to ensure effectively removing



**Fig. 2** Schematic diagram of the three different scanning paths: **a** LTCS, **b** FTSS, **c** FLCS

**Fig. 3** Schematic diagram of the laser scanning parameters



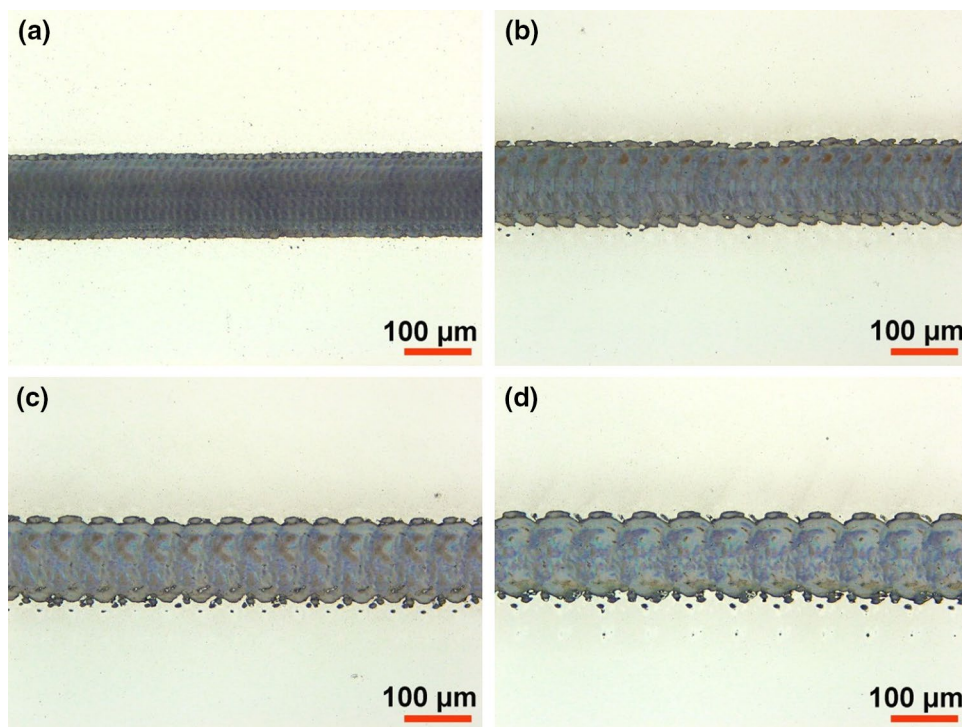
the unwanted Ag film as much as possible, the  $v$  and  $HD$  values could not be high during the SLA process. This was due to the fact that the higher  $v$  and  $HD$  values could lead to more irradiation-free zones which would finally form residues and thus deteriorate the edge quality [17].

Figure 4 shows the top-view images of laser-ablated grooves at various  $v$  values obtained from CLSM system. It was seen that Ag films were successfully detached from the glass substrates after laser ablation. Here, the laser ablation mechanism can be explained by the generation of the well-known laser-induced thermo-elastic force and the partial vaporization of the film material. The thermo-elastic force, which plays a main role to desorb the film from the substrate when it exceeds the cohesion of the film and its adhesion to the substrate, is generated by rapid thermal expansion resulting from the ns pulsed laser irradiation [25–28]. The thermo-elastic force is proportional to the rate of temperature increase, and not determined by the absolute magnitude of temperature rise [25, 26]. Therefore, laser patterning of a thin film without reaching the melting point is possible when the laser-induced thermo-elastic force exceeds a pulse energy density threshold. However, when the laser-induced thermo-elastic force is below the pulse energy density threshold, the removal mechanism is mainly attributed to partial vaporization of the thin film. The partial vaporization of metal films is a photo-thermal process in which the surface material will be rapidly heated and vaporized from the substrate [11, 12]. It was observed in Fig. 4a that the laser spot diameter irradiated on the Ag film surface was

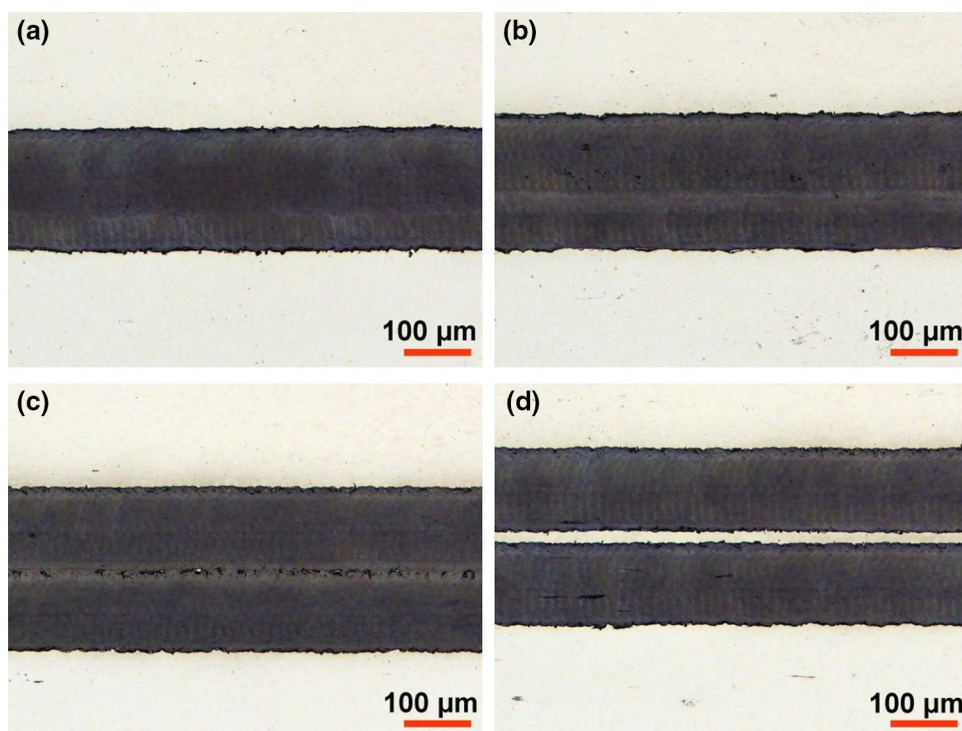
130  $\mu\text{m}$  under the condition of using a defocusing amount of 1.0 mm and a laser fluence of  $0.8 \text{ J}/\text{cm}^2$ . When the  $v$  value further increased, the difference in ablated groove width did not change significantly. More interestingly, the edge of the laser-ablated grooves gradually became unsmooth and exhibited semicircle-shaped boundaries when the  $v$  value increased from 15 to 75 mm/s in increments of 20 mm/s, and the same phenomenon can be found in [29]. This result may be attributed to different laser pulse distributions at different  $v$  values, since the increase of  $v$  value led to a decrease of the laser spot overlapping rate ( $SO_R$ ) which means a smaller effective ablation area [30, 31]. When the low  $v$  value of 15 mm/s was adopted, two adjacent laser spots generated a large overlapping area, which was conducive to eliminating the semicircle-shaped boundaries of the laser-irradiated zone. As a consequence, a straight groove with smooth edges was formed, as shown in Fig. 4a. On the contrary, the increase of  $v$  value resulted in a decreased overlapping area of two adjacent laser spots and thus the formation of slightly unsmooth edges with semicircle-shaped boundaries and Ag residues [32, 33], as can be seen in Fig. 4b–d. Therefore, an ablated groove with good edge quality can be produced under the  $v$  value of 15 mm/s and this result is consistent with the above theoretical analysis about the  $v$  value.

Figure 5 illustrates the CLSM images of the SLA patterns at a constant  $v$  value of 15 mm/s and various  $HD$  values (i.e. 50  $\mu\text{m}$ , 90  $\mu\text{m}$ , 130  $\mu\text{m}$ , and 170  $\mu\text{m}$ ). It was found that when  $HD$  increased from 50 to 90  $\mu\text{m}$ , the pattern width increased from 180 to 210  $\mu\text{m}$  and straight grooves without

**Fig. 4** CLSM images of the laser-ablated grooves on Ag films at  $v$  values of **a** 15 mm/s, **b** 35 mm/s, **c** 55 mm/s and **d** 75 mm/s



**Fig. 5** CLSM images of the SLA patterns on Ag films at a constant  $v$  value of 15 mm/s and  $HD$  values of **a** 50  $\mu\text{m}$ , **b** 90  $\mu\text{m}$ , **c** 130  $\mu\text{m}$  and **d** 170  $\mu\text{m}$



material residues were formed (Fig. 5a, b). Increasing  $HD$  to 130  $\mu\text{m}$  that represented the condition in which the laser spots were tangent to produce two adjacent grooves, some Ag residues occurred at the center of the pattern (Fig. 5c). Further increasing  $HD$  to 170  $\mu\text{m}$ , two parallel grooves separated by an Ag ridge were formed (Fig. 5d). This may be due to the fact that the irradiation-free zones, which will finally turn to material residues or ridges, between two adjacent grooves increased as the increase of  $HD$  [33, 34].

Figure 6 shows the schematic diagram of the SLA patterns obtained by using different  $HD$  values. When  $HD$  is smaller than the laser spot diameter (130  $\mu\text{m}$ ), the adjacent laser scanning tracks are overlapped, leading to no irradiation-free zone between two adjacent tracks [35]. As a result, smooth patterns with good edge quality and no Ag residues

are generated, as revealed in Fig. 6a. However, the ablation efficiency is low in this condition, i.e. more time is needed in processing an area with the same size. When  $HD$  increases to 130  $\mu\text{m}$ , as Fig. 6b shows, the adjacent laser scanning tracks are tangent to each other and some irradiation-free zones (marked by red circles in Fig. 6b) occur. In these irradiation-free zones, the Ag film will not undergo laser ablation and remain on the surface which will finally turn to Ag residues and lower the surface quality. As shown in Fig. 5c, further increasing  $HD$  to 170  $\mu\text{m}$ , the adjacent laser scanning tracks become parallel and are separated by the middle Ag ridge-like residues. Tang et al. [22] and Yang et al. [36] fabricated organized structures on copper and titanium alloy by laser scanning under this condition, and achieved high-efficiency processing with poor surface quality. Based on the

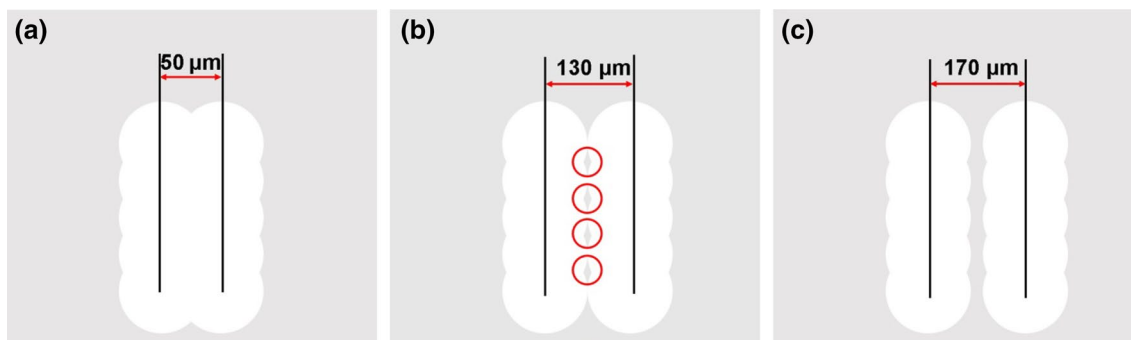


**Fig. 6** Schematic diagram of the SLA patterns at different  $HD$  values: **a** 50  $\mu\text{m}$ , **b** 130  $\mu\text{m}$ , **c** 170  $\mu\text{m}$

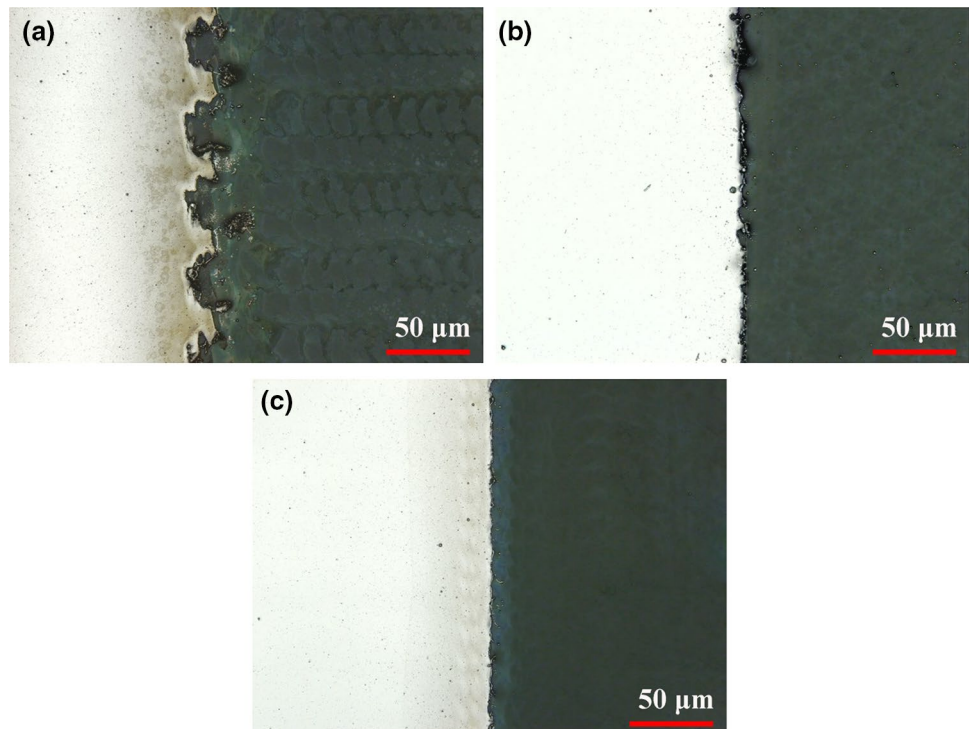
above analysis, there must be a trade-off between ablation efficiency and  $HD$  since high  $HD$  will lead to high ablation efficiency and poor surface quality [21].

In order to confirm the truth that the proposed scanning paths can improve the edge quality of SLA patterns, the edges under different scanning paths were compared. Figure 7 exhibits the CLSM images of the edges of SLA patterns obtained by using scanning paths of LTCS, FTSS and FLCS. Considering both ablation efficiency and edge quality, the  $v$  and  $HD$  values were set to 15 mm/s and 90  $\mu\text{m}$ , respectively. As Fig. 7a shows, when the conventional LTCS was adopted, the edge was unsmooth and slightly yellowed. This should be attributed to that the start and end points of laser scanning involve a longer action time than other points, and thus more laser energy will be exerted on the Ag film. This huge amount of energy was delivered into the Ag film and led to the formation of oxide, resulting in the formation of the yellow areas around the laser-ablated patterns in the optical image [1, 5, 37]. On the other hand, the start and end areas of the laser scanning track are usually semicircle-shaped due to the influence of the laser spot projection [38]. Combined with these two factors, unsmooth and slightly yellowed edges will finally generated during SLA, as indicated in the report of Tang et al. [22]. According to the above discussion about laser-ablated grooves and SLA patterns, the middle part of the laser-ablated groove is relatively clean and smooth under the condition of using a  $v$  value of 15 mm/s and an  $HD$  value below 130  $\mu\text{m}$ . Therefore, the edge quality can be effectively improved by using

the smooth middle part to pattern Ag films combined with an outer laser-ablated frame to determine the boundary with less thermal effect. The proposed strategies of FTSS and FLCS were just based on this guideline. For the FTSS, the Ag film was ablated along the outer frame to the predetermined depth firstly and then successively along the inner frames with gradually decreased sizes. In the case of the FLCS, the initial shape of the pattern was firstly formed through the conventional LTCS, and then the unsmooth part of the edge was further eliminated by laser ablation along the outer frame. Thereupon, smooth edges with no obvious heat-affected zone could be formed, as shown in Fig. 7b, c.

Figure 8 shows the CLSM three-dimensional profiles of the laser-ablated areas obtained by using scanning paths of LTCS, FTSS and FLCS with a  $v$  value of 15 mm/s and an  $HD$  value of 90  $\mu\text{m}$ . It was clearly seen that in the cases of the FTSS and FLCS (Fig. 8b, c), the edges were much smoother than that for the conventional LTCS (Fig. 8a) which was featured by uneven boundaries with much more Ag residues [38]. This result is consistent with the above analysis. It was also worth noting that the edges of all patterns had some obvious protuberances, which may be ascribed to the edge peeling of the Ag film. The thermo-elastic force generated by laser irradiation on the edge part was lower than the cohesion of the film and its adhesion to the substrate owing to the Gaussian energy distribution of the ns laser pulses [39, 40], and therefore the Ag film at the edge was hard to be desorbed from the substrate. Differently, the thermo-elastic force generated on the middle part

**Fig. 7** CLSM images of the edges of SLA patterns on Ag films with an area of 1.0 mm  $\times$  1.0 mm at a  $v$  value of 15 mm/s and an  $HD$  value of 90  $\mu\text{m}$  using scanning paths of **a** LTCS, **b** FTSS and **c** FLCS



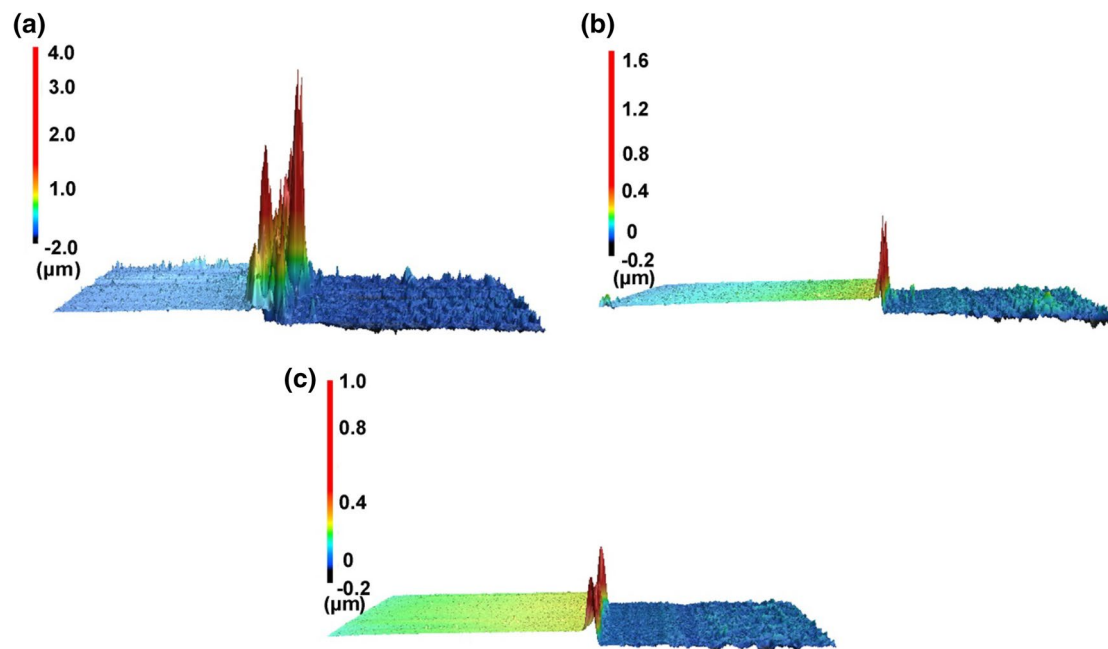


**Fig. 8** CLSM three-dimensional profiles of the laser-ablated areas on Ag films at a  $v$  value of 15 mm/s and an  $HD$  value of 90  $\mu\text{m}$  using scanning paths of **a** LTCS, **b** FTSS and **c** FLCS

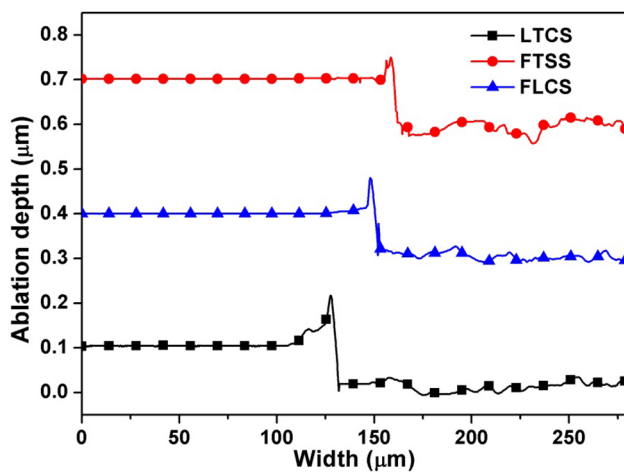


**Fig. 9** Cross-sections of the laser-ablated patterns at a  $v$  value of 15 mm/s and an  $HD$  value of 90  $\mu\text{m}$  using scanning paths of LTCS, FTSS and FLCS

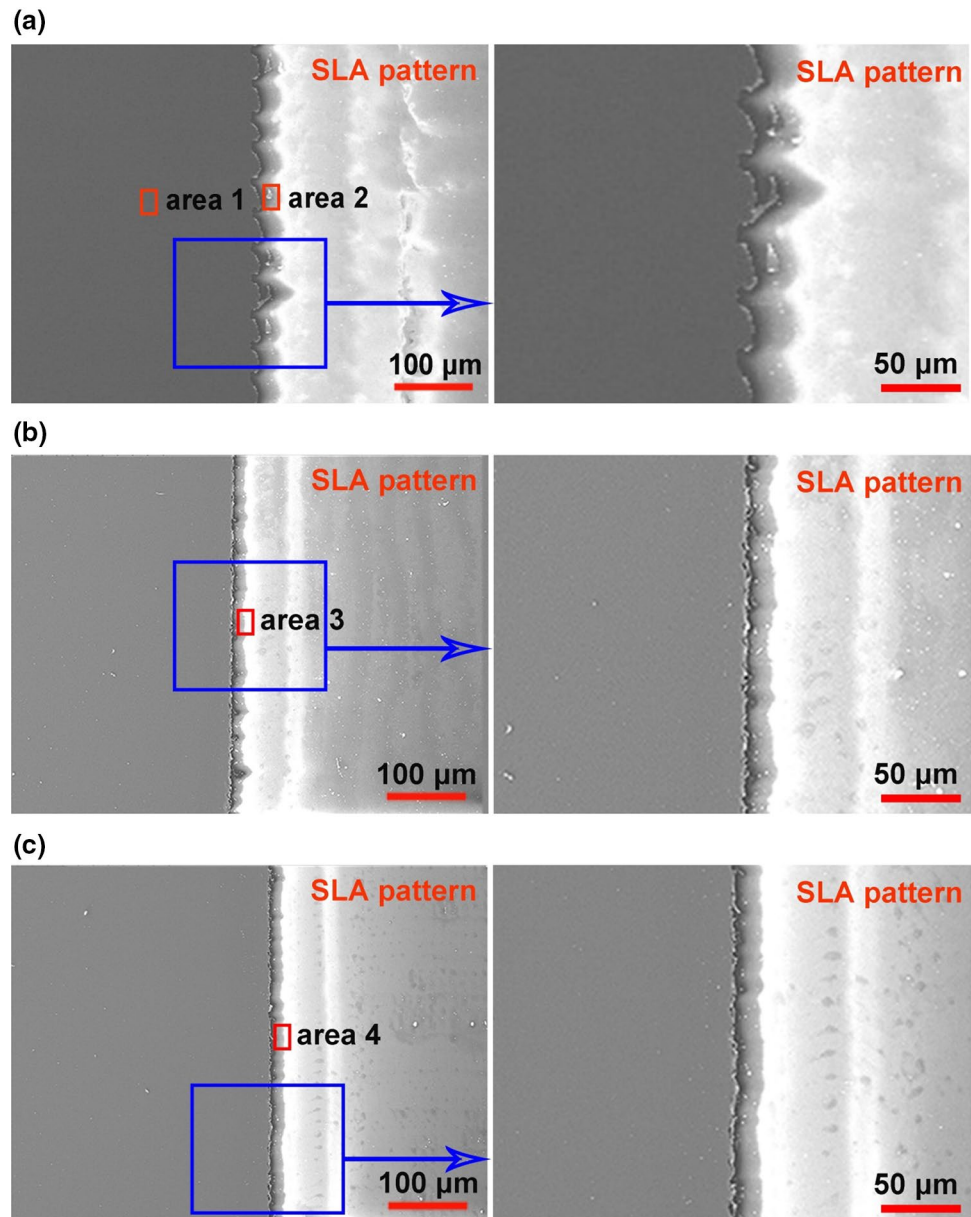
of the laser-irradiated zone was high enough to desorb the Ag film from the substrate. When the Ag film at the middle part was desorbed from the substrate, the remained Ag film at the edge formed the protuberance morphology.

The cross-sections of laser-ablated patterns with different scanning paths are shown in Fig. 9. It could be seen that the effective ablation depth of all the ablated patterns was approximately 100 nm, which implied that the Ag film was almost completely removed without generating obvious damage to the glass substrate [6, 41]. Also ridge-like profiles

were found at the edge of all the ablated patterns. However, the ridge heights of the ablated patterns obtained by using the scanning paths of FTSS and FLCS were obviously lower as compared with LTCS. The result is consistent with the foregoing discussion about the CLSM three-dimensional profiles of the laser-ablated patterns.

Figure 10 shows the low magnification (left) and local enlarged (right) SEM images of the edges of SLA patterns obtained by using the scanning paths of LTCS, FTSS and FLCS. As exhibited in Fig. 10a, the edge obtained by using the scanning path of LTCS was semicircle-shaped with some obvious Ag material residues, which can be obviously seen from the local enlarged image. The Ag residues was originated from the Gaussian distribution of the ns laser pulses, which led to the relatively low laser-induced thermo-elastic force at the periphery of the laser-irradiated zone that below the pulse energy density threshold [39, 40]. Therefore, the main removal mechanism at the periphery of the laser-irradiated zone was attributed to partial vaporization of the Ag film. The energy absorbed by the Ag film at the periphery could only realize partial ablation of the Ag film, and the unablated Ag would finally turn to materials residues. Interestingly, the edge obtained by using the scanning paths of FTSS and FLCS, as Fig. 10b, c reveal, was much smoother and no obvious material residues could be found. This should be ascribed to the fact that the Ag film at the periphery could be effectively removed under the scanning path of FTSS or FLCS owing to the higher laser spot overlapping rate ( $SO_R$ ) at the edge of the laser-irradiated zone.

**Fig. 10** Low magnification (left) and local enlarged (right) SEM images of the edges of SLA patterns on Ag films at a  $v$  value of 15 mm/s and an  $HD$  value of 90  $\mu\text{m}$  using scanning paths of **a** LTCS, **b** FTSS and **c** FLCS. The rectangle-marked areas 1–4 represent the EDX analysis areas



This result is completely consistent with the above CLSM analysis. From these results, it is confirmed that SLA patterns with good edge quality can be generated by introducing the scanning path of FTSS or FLCS under the condition of using a  $v$  value of 15 mm/s and an  $HD$  value of 90  $\mu\text{m}$ .

In order to further confirm that the edge quality could be effectively improved by introducing the scanning path of FTSS or FLCS, an EDX spectrometer was used to investigate the phase composition changes at the Ag film surfaces and the edges of SLA patterns on Ag films under different scanning paths [41]. The EDX results with the atomic percent (at%) of each element for the areas 1–4 marked by rectangles in Fig. 10a–c are shown in Fig. 11. The EDX spectrum for the unablated zone of the Ag film, as shown

in Fig. 11a, revealed that the sample contained silver (Ag), silicon (Si), oxygen (O), sodium (Na), calcium (Ca), magnesium (Mg) and aluminum (Al) elements. The Ag element was originated from the Ag film, and the presence of all the other elements was ascribed to the use of the glass substrate. The same result has also been reported by Sonal et al. [42]. Clear observation was that the atomic percent of Ag element changed from 33.25 to 0.56% after SLA using the scanning path of the conventional LTCS (Fig. 11b), indicating that the LTCS was disadvantaged in entirely removing the Ag film and thus produced some Ag residues at the edge of the laser ablation zone. Interestingly, the atomic percent of Ag element changed to 0% after SLA using the scanning paths of FTSS (Fig. 11c) and FLCS (Fig. 11d). These results further



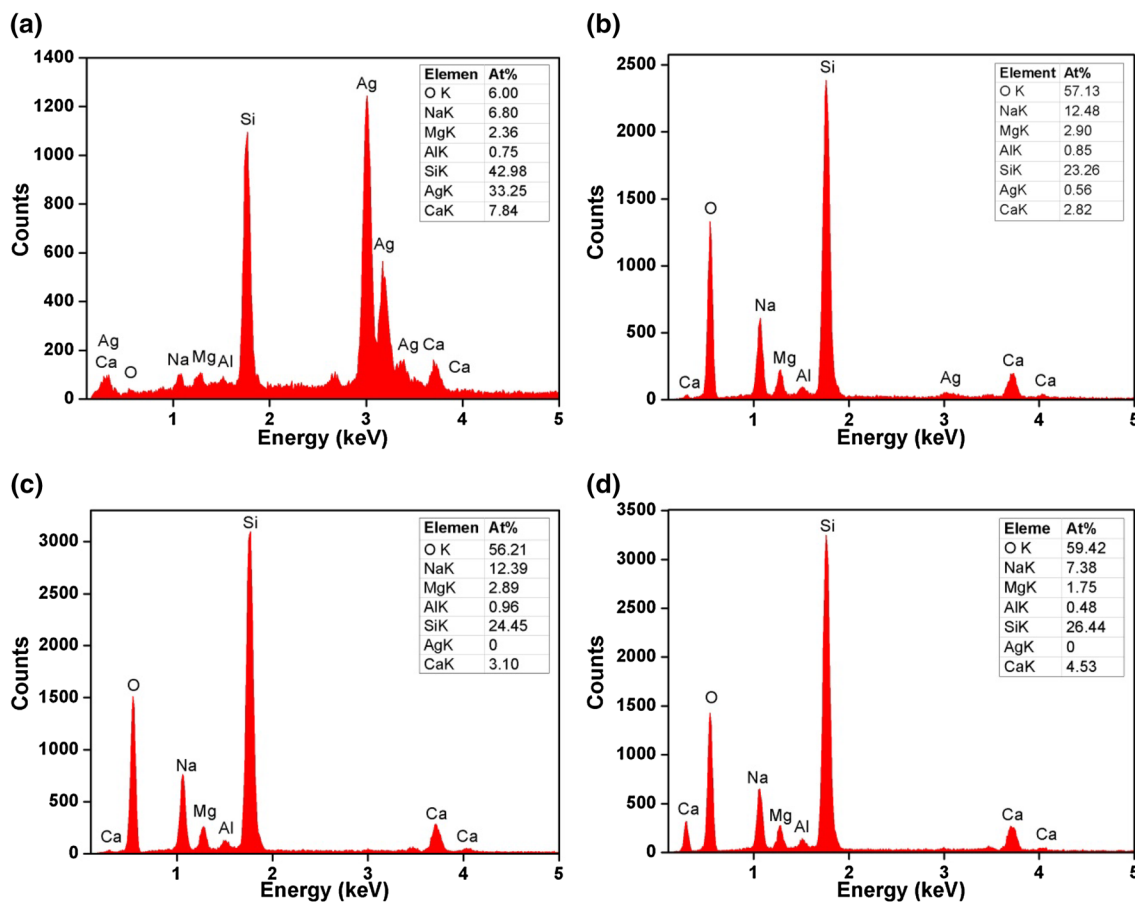


**Fig. 11** EDX spectra with atomic percent data showing chemical compositions of **a** area 1, **b** area 2, **c** area 3 and **d** area 4 marked in Fig. 10a–c

confirmed that there were no Ag residues around the edge when the proposed scanning paths of FTSS and FLCS were employed.

SLA patterns with the same area of 10 mm × 10 mm were prepared under the scanning paths of LTCS, FTSS and FLCS to verify the efficacy of the proposed scanning paths of FTSS and FLCS on improving the optical transmittance. Figure 12 shows the optical transmittance spectra of the glass substrate, the original Ag/glass sample and the SLA patterned Ag/glass samples prepared by using various scanning paths. The optical transmittance of the glass substrate was about 97% over the visible range of wavelength. After magnetron sputtering deposition of a 100-nm-thick Ag layer, the optical transmittance of the Ag/glass was very low and an obvious absorption peak was observed in the wavelength range of 300–350 nm. This phenomenon should be attributed to the fact that the Ag film has high light absorption in the short wavelength region [43–45]. All the SLA patterned Ag/glass samples displayed significantly increased optical transmittances due to the partial removal of the Ag films. However, the optical transmittances of the SLA patterned Ag/glass samples prepared by using the scanning paths of FTSS and

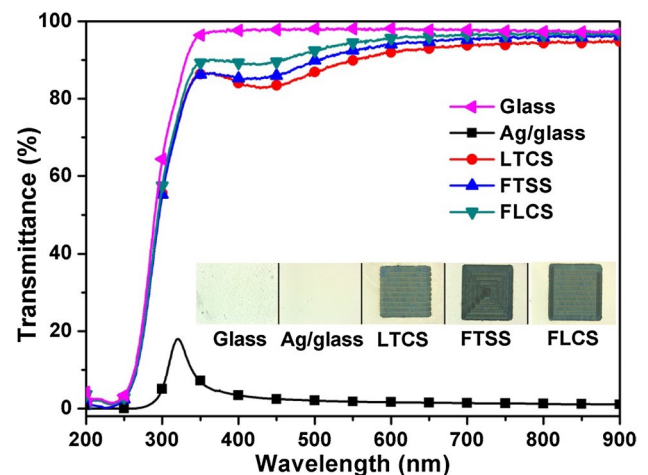


**Fig. 12** Optical transmittance spectra of SLA patterned Ag/glass samples with an area of 1.0 mm × 1.0 mm prepared at a  $v$  value of 15 mm/s and an  $HD$  value of 90  $\mu$ m using scanning paths of LTCS, FTSS and FLCS. The optical transmittance spectra of the glass substrate and the original Ag/glass sample are provided for comparison. The insets show the glass substrate, the Ag/glass and the SLA patterned Ag/glass under different scanning paths

FLCS were found to be relatively higher as compared to that of the SLA patterned Ag/glass sample prepared by using the scanning path of LTCS. It is commonly believed that the complete removal of the Ag layer with fewer residues can significantly improve the optical transmittance, i.e. the fewer the Ag residues, the higher the optical transmittance. As mentioned above, adopting the scanning paths of FTSS and FLCS effectively reduced the Ag residues, which should be responsible for the relatively higher optical transmittances. It also can be observed that no matter what kind of scanning path was used, all the SLA patterns exhibited the broad absorption dips centered at  $\sim 450$  nm, which should be ascribed to the localized surface plasmon resonance (LSPR) of Ag residues [46]. Domingues et al. [47] reported that the growing in number of Ag residues would increase the intensity of the LSPR band, characterized by a decrease of the transmittance minimum. Since the use of the scanning paths of FTSS and FLCS resulted in relatively higher optical transmittance minimum values centered at  $\sim 450$  nm compared to the LTCS, it was confirmed that the FTSS and FLCS could be more effective for eliminating the Ag residues. The insets in Fig. 12 show that after laser ablation, square SLA patterns were formed on the surfaces of the samples obtained by LTCS, FTSS and FLCS. Interestingly, the partial edge of the SLA patterns under the traditional scanning path of LTCS was uneven and exhibited semicircle-shaped boundaries, while the edges of the SLA patterns obtained by FTSS and FLCS were smooth, which are consistent with the previous results. All the results suggest the effectiveness of the proposed scanning methods of adopting FTSS and FLCS in improving the edge quality and the optical transmittance of SLA Ag patterns, which may have a great potential application in the fields that demand good edge quality and even high transparency of laser-ablated metal films.

## 4 Conclusions

In summary, we proposed two new scanning methods, which using simple scanning paths of FTSS and FLCS, for improving the edge quality during SLA of Ag films deposited on glass substrates by RF magnetron sputtering. The effects of  $v$  and  $HD$  values on edge quality of laser-ablated grooves and patterns were firstly studied to determine the optimal laser scanning parameters for SLA. Then the effects of the conventional LTCS and the proposed FTSS and FLCS on edge quality and optical transmittance of SLA patterns were comparatively analyzed under the optimal laser scanning parameters. It was found that the high  $v$  and  $HD$  values resulted in poor edge quality, and the optimal  $v$  and  $HD$  values were respectively 15 mm/s and 90  $\mu\text{m}$  in the present work. Unlike the unsmooth edge with semicircle-shaped boundaries and some Ag residues obtained by using the

conventional LTCS, the edges obtained by using FTSS and FLCS were relatively smooth without obvious heat-affected zone and Ag residues, resulting in relatively high optical transmittances. These results confirmed the availability of the proposed scanning methods of adopting the FTSS and FLCS in effectively improving the edge quality and even the optical transmittance of SLA Ag patterns. This study may have great potential application in various fields such as laser cleaning, laser polishing, scribing/grooving of solar modules and preparation of metal mesh structures.

**Acknowledgements** This work was funded by the National Natural Science Foundation of China (Grant Nos. 51805220 and 61405078), the Natural Science Foundation of Jiangsu Province of China (Grant No. BK20140567) and the Jiangsu University Study-abroad Fund (Reference No. UJS-2017-013). The authors would like to thank the support of the Young Backbone Teacher Cultivating Project of Jiangsu University.

## References

1. C.J. Hayden, C. Dalton, Direct patterning of microelectrode arrays using femtosecond laser micromachining. *Appl. Surf. Sci.* **256**, 3761–3766 (2010)
2. S. Liébana, L.J. Jones, G.A. Drago, R.W. Pittson, D. Perrie, J.P. Hart, Design and development of novel screen-printed microelectrode and microbiosensor arrays fabricated using ultrafast pulsed laser ablation. *Sens. Actuators, B* **231**, 384–392 (2016)
3. H. Yu, H. Lee, J. Lee, H. Shin, M. Lee, Laser-assisted patterning of solution-processed oxide semiconductor thin film using a metal absorption layer. *Microelectron. Eng.* **88**, 6–10 (2011)
4. T. Hassinen, T. Ruotsalainen, P. Laakso, R. Penttilä, H.G.O. Sandberg, Roll-to-roll compatible organic thin film transistor manufacturing technique by printing, lamination, and laser ablation. *Thin Solid Films* **571**, 212–217 (2014)
5. K. Zhao, Z.Y. Jia, J.W. Ma, W. Liu, L. Wang, Nanosecond multi-pulse laser milling for certain area removal of metal coating on plastics surface. *Opt. Lasers Eng.* **63**, 58–69 (2014)
6. N. Farid, H. Chan, D. Milne, A. Brunton, G.M. O'Connor, Stress assisted selective ablation of ITO thin film by picosecond laser. *Appl. Surf. Sci.* **427**, 499–504 (2018)
7. P.V.D. Weijer, P.C.P. Bouten, H. Fledderus, R.R. Janssen, S.H.P.M.D. Winter, H.B. Akkerman, Mechanistic study on black and grey spot growth in OLEDs performed on laser-ablated pinholes in the cathode. *Org. Electron.* **42**, 59–65 (2017)
8. D. Walter, A. Fell, E. Franklin, D. Wang, K. Fong, K. Teng, K. Weber, A.W. Blakers, Damage-free ultraviolet nanosecond laser ablation for high efficiency back contact solar cell fabrication. *Sol. Energy Mater. Sol. Cells* **136**, 1–10 (2015)
9. S. Harrison, O. Nos, G. D'Alonzo, C. Denis, A. Coll, D. Munoz, Back contact heterojunction solar cells patterned by laser ablation. *Energy Procedia* **92**, 730–737 (2016)
10. S. Ring, S. Kirner, C. Schultz, P. Sonntag, B. Stannowski, L. Korte, R. Schlatmann, Emitter patterning for back-contacted Si heterojunction solar cells using laser written mask layers for etching and self-aligned passivation (LEAP). *IEEE J. Photovoltaics* **6**, 894–899 (2016)
11. G. Heise, M. Englmaier, C. Hellwig, T. Kuznicki, S. Sarrach, H.P. Huber, Laser ablation of thin molybdenum films on transparent substrates at low fluences. *Appl. Phys. A* **102**, 173–178 (2011)

12. N. Lasemi, U. Pacher, L.V. Zhigilei, O. Bomati-Miguel, R. Lahoz, W. Kautek, Pulsed laser ablation and incubation of nickel, iron and tungsten in liquids and air. *Appl. Surf. Sci.* **433**, 772–779 (2018)
13. K. Trabelsi, A. Hajjaji, I. Ka, M. Gaidi, B. Bessais, M.A.E.I. Khakani, Optoelectronic and photocatalytic properties of in situ platinum-doped TiO<sub>2</sub> films deposited by means of pulsed laser ablation technique. *J. Mater. Sci.* **28**, 3317–3324 (2017)
14. G. Heise, M. Dickmann, M. Domke, A. Heiss, T. Kuznicki, J. Palm, I. Richter, Investigation of the ablation of zinc oxide thin films on copper-indium-selenide layers by ps laser pulses. *Appl. Phys. A* **104**, 387–393 (2011)
15. Y. Shi, Z. Wu, L. Du, S. Li, Y. Jiang, Effect of the thickness of Si film on Si/Se film doped silicon prepared by femtosecond laser. *J. Mater. Sci.* **29**, 4526–4532 (2018)
16. G. Heise, M. Domke, J. Konrad, S. Sarrach, J. Sotrop, H.P. Huber, Laser lift-off initiated by direct induced ablation of different metal thin films with ultra-short laser pulses. *J. Appl. Phys.* **45**, 315303 (2012)
17. G. Tang, A.C. Hourd, A. Abdolvand, Nanosecond pulsed laser blackening of copper. *Appl. Phys. Lett.* **101**, 231902 (2012)
18. H. Yoo, H. Shin, M. Lee, Direct patterning of double-layered metal thin films by a pulsed Nd:YAG laser beam. *Thin Solid Films* **518**, 2775–2778 (2010)
19. H. Lee, H. Shin, Y. Jeong, J. Moon, M. Lee, Laser-direct photoetching of metal thin film for the electrode of transistor. *Appl. Phys. Lett.* **95**, 071104 (2009)
20. H. Yu, H. Shin, M. Lee, Single-step fabrication of double-layered metal thin film pattern for the electrodes of electronic devices. *Curr. Appl. Phys.* **11**, S179–S182 (2011)
21. L. Romoli, M.M.A. Khan, M. Valentini, Through-the-thickness selective laser ablation of ceramic coatings on soda-lime glass. *Opt. Laser Technol.* **90**, 113–121 (2017)
22. G. Tang, A. Abdolvand, Laser-assisted highly organized structuring of copper. *Opt. Mater. Express* **1**, 1425–1432 (2011)
23. S. Richards, M.A. Baker, M.D. Wilson, A. Lohstroh, P. Seller, Femtosecond laser ablation of cadmium tungstate for scintillator arrays. *Opt. Lasers Eng.* **83**, 116–125 (2016)
24. E. Williams, E.B. Brousseau, A. Rees, Nanosecond Yb fibre laser milling of aluminium: effect of process parameters on the achievable surface finish and machining efficiency. *Int. J. Adv. Manuf. Technol.* **74**, 769–780 (2014)
25. M. Arronte, P. Neves, R. Vilar, Modeling of laser cleaning of metallic particulate contaminants from silicon surfaces. *J. Appl. Phys.* **92**, 6973–6982 (2002)
26. J.M. Lee, C. Curran, K.G. Watkins, Laser removal of copper particles from silicon wafers using UV, visible and IR radiation. *Appl. Phys. A* **73**, 219–224 (2001)
27. G. Vereecke, E. Rohr, M.M. Heyns, Laser-assisted removal of particles on silicon wafers. *J. Appl. Phys.* **85**, 3837–3843 (1999)
28. K. Wu, Y. Xia, H.Z. Yuan, J.Y. Zhang, G. Liu, J. Sun, Cohesive and adhesive properties of nanocrystalline Ti thin films on polyimide substrates. *Mater. Sci. Eng. A* **744**, 746–753 (2019)
29. H.J. Kim, K.W. Seo, H.K. Yong, J. Choi, H.K. Kim, Direct laser patterning of transparent ITO–Ag–ITO multilayer anodes for organic solar cells. *Appl. Surf. Sci.* **328**, 215–221 (2015)
30. L.J. Huang, B.J. Li, N.F. Ren, Enhancing optical and electrical properties of Al-doped ZnO coated polyethylene terephthalate substrates by laser annealing using overlap rate controlling strategy. *Ceram. Int.* **42**, 7246–7252 (2016)
31. A.H.A. Lutey, A. Fortunato, A. Ascari, S. Carmignato, C. Leone, Laser cutting of lithium iron phosphate battery electrodes: characterization of process efficiency and quality. *Opt. Laser Technol.* **65**, 164–174 (2015)
32. J. Shi, H. Wang, D. Zhang, F. Chen, X. Yao, Femtosecond laser directly writing microholes in Bi(Nb<sub>0.998</sub>V<sub>0.002</sub>)O<sub>4</sub> ceramic and multi-photon induced large scale nanometer wires array. *J. Mater. Sci.* **22**, 1–5 (2011)
33. G. Tang, A. Abdolvand, Structuring of titanium using a nano-second-pulsed Nd:YVO<sub>4</sub> laser at 1064 nm. *Int. J. Adv. Manuf. Technol.* **66**, 1769–1775 (2013)
34. P. Knotek, J. Navesnik, T. Cernohorsky, M. Kincl, M. Vlcek, L. Tichy, Ablation of (GeS<sub>2</sub>)<sub>0.3</sub>(Sb<sub>2</sub>S<sub>3</sub>)<sub>0.7</sub> glass with an ultra-violet nano-second laser. *Mater. Res. Bull.* **64**, 42–50 (2015)
35. B.Y. Wu, P. Liu, J. Duan, L.M. Deng, X.Y. Zeng, X.Z. Wang, Study on picosecond pulse laser ablation of Cr12MoV cold work mold steel. *Mater. Des.* **110**, 549–557 (2016)
36. C.C. Yang, Y.C. Lin, C.C. Yang, Y.H. Lin, K.C. Huang, K.M. Lin, W.T. Hsiao, Laser-induced coloring of titanium alloy using ultra-violet nanosecond pulses scanning technology. *J. Alloys Compd.* **715**, 349–361 (2017)
37. A. Latif, M.S. Rafiq, K.A. Bhatti, A. Perveen, Crater geometry and morphological changes on gold sheet during laser microdrilling. *Int. J. Adv. Manuf. Technol.* **85**, 2847–2855 (2016)
38. P. Umenne, V.V. Srinivasu, Femtosecond-laser fabrication of micron and sub-micron sized S-shaped constrictions on high T<sub>c</sub> superconducting YBa<sub>2</sub>Cu<sub>3</sub>O<sub>7-x</sub> thin films: ablation and lithography issues. *J. Mater. Sci.* **28**, 5817–5826 (2017)
39. F. Abrinaei, M. Shirazi, Nonlinear optical investigations on Al doping ratio in ZnO thin film under pulsed Nd:YAG laser irradiation. *J. Mater. Sci.* **28**, 17541–17550 (2017)
40. M.A. Morsi, A. Rajeh, A.A. Menazea, Nanosecond laser-irradiation assisted the improvement of structural, optical and thermal properties of polyvinyl pyrrolidone/carboxymethyl cellulose blend filled with gold nanoparticles. *J. Mater. Sci.* **30**, 2693–2705 (2019)
41. H.Y. Kim, J.W. Yoon, W.S. Choi, K.R. Kim, S.H. Cho, Ablation depth control with 40 nm resolution on ITO thin films using a square, flat top beam shaped femtosecond NIR laser. *Opt. Lasers Eng.* **84**, 44–50 (2016)
42. A. Sonal, S. Sharma, Aggarwal, Optical investigation of soda lime glass with buried silver nanoparticles synthesised by ion implantation. *J. Non-Cryst. Solids* **485**, 57–65 (2018)
43. B.J. Li, G.Y. Yang, L.J. Huang, W. Zu, H. Li, Y.L. Wang, S.S. Li, N.F. Ren, Surface morphology and photoelectric properties of FTO ceramic thin films under a simple transparent cover-assisted laser annealing. *Mater. Res. Bull.* **108**, 151–155 (2018)
44. L.J. Huang, N.F. Ren, B.J. Li, M. Zhou, Improvement in overall photoelectric properties of Ag/FTO bilayer thin films using furnace/laser dual annealing. *Mater. Lett.* **116**, 405–407 (2014)
45. B.J. Li, H. Li, L.J. Huang, H.D. Cao, W. Zu, N.F. Ren, H. Ding, X. Kong, J.L. Zhang, Performance optimization of fluorine-doped tin oxide thin films by introducing ultrasonic vibration during laser annealing. *Ceram. Int.* **43**, 7329–7337 (2017)
46. J. Huang, X. Liu, Y. Lu, Y. Zhou, J. Xu, J. Li, H. Wang, J. Fang, Y. Yang, W. Wang, R. Tan, W. Song, Seed-layer-free growth of ultra-thin Ag transparent conductive films imparts flexibility to polymer solar cells. *Sol. Energy Mater. Sol. Cells* **184**, 73–81 (2018)
47. R.P. Domingues, M.S. Rodrigues, M. Proença, D. Costa, E. Alves, N.P. Barradas, F.J. Oliveira, R.F. Silva, J. Borges, F. Vaz, Thin films composed of Au nanoparticles embedded in AlN: influence of metal concentration and thermal annealing on the LSPR band. *Vacuum* **157**, 414–421 (2018)